





# In situ visualization of loading-dependent water effects in a stable metal–organic framework

Nicholas C. Burtch <sup>1,5</sup>, Ian M. Walton<sup>1,5</sup>, Julian T. Hungerford<sup>1</sup>, Cody R. Morelock<sup>1</sup>, Yang Jiao <sup>1</sup>, Jurn Heinen<sup>2</sup>, Yu-Sheng Chen<sup>3</sup>, Andrey A. Yakovenko<sup>4</sup>, Wenqian Xu<sup>4</sup>, David Dubbeldam <sup>2</sup> and Krista S. Walton <sup>1\*</sup>

*Nature Chemistry* 12, 186–192(2020) | [Cite this article](#)

7618 Accesses | 10 Altmetric | [Metrics](#)

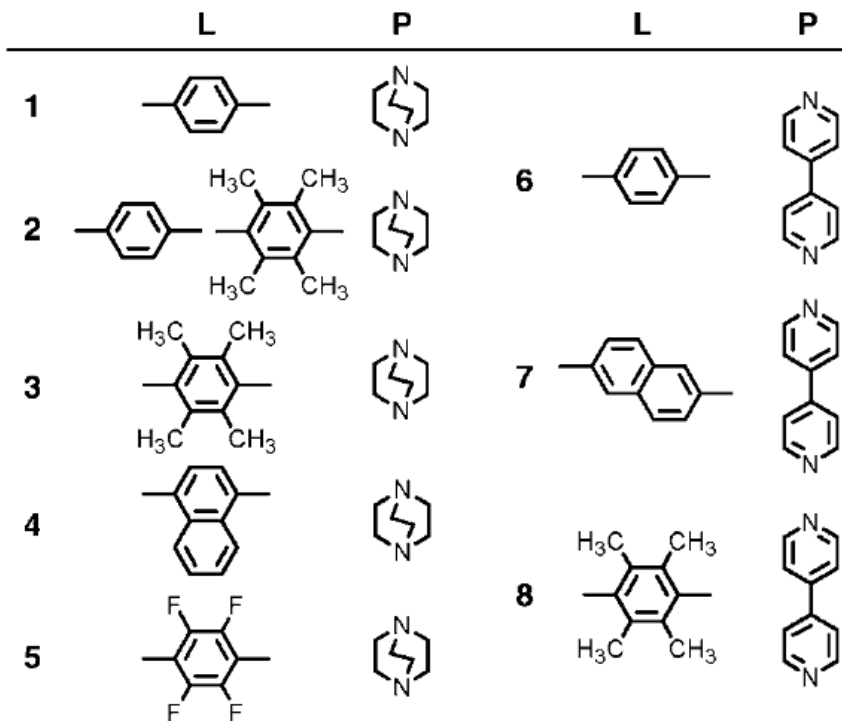
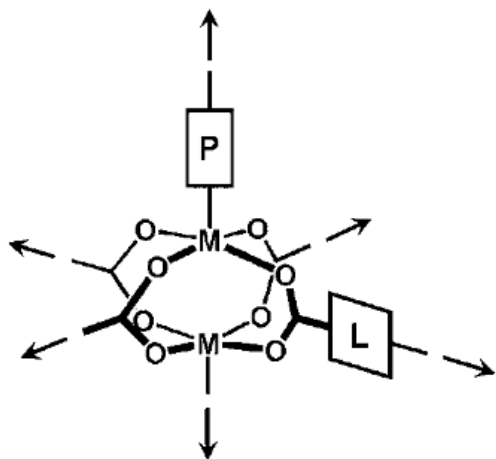
**Paper presentation**

**16<sup>th</sup> Group meeting**

**23-05-2020**

- Ankit Nagar

# Background



Scheme 1. Linkers (L) and pillars (P) in paddle-wheel-based nets 1–8.

*Chem. Eur. J.* **2005**, *11*, 3521 – 3529

# Relevance to the group

- Microstrain behavior of MOFs and clusters studied through powder diffraction.
- Adsorption behavior of hydrogels

# Introduction

- The impact of water interactions on the structural properties of stable MOFs remains largely unknown
- Crystallographic evidence of the importance of loading-dependent water effects on the structural properties of a water stable MOF that does not undergo large-scale structural transitions upon interactions with water.
- A series of *in situ* synchrotron X-ray diffraction (XRD) experiments, infrared (IR) spectroscopy and molecular simulation analysis on the DMOF-TM framework,  $Zn_2(BDC-TM)_2(DABCO)$   
(**BDC-TM**=2,3,5,6-tetramethyl-1,4-benzenedicarboxylic acid,  
**DABCO**=1,4 diazabicyclo[2.2.2]octane)

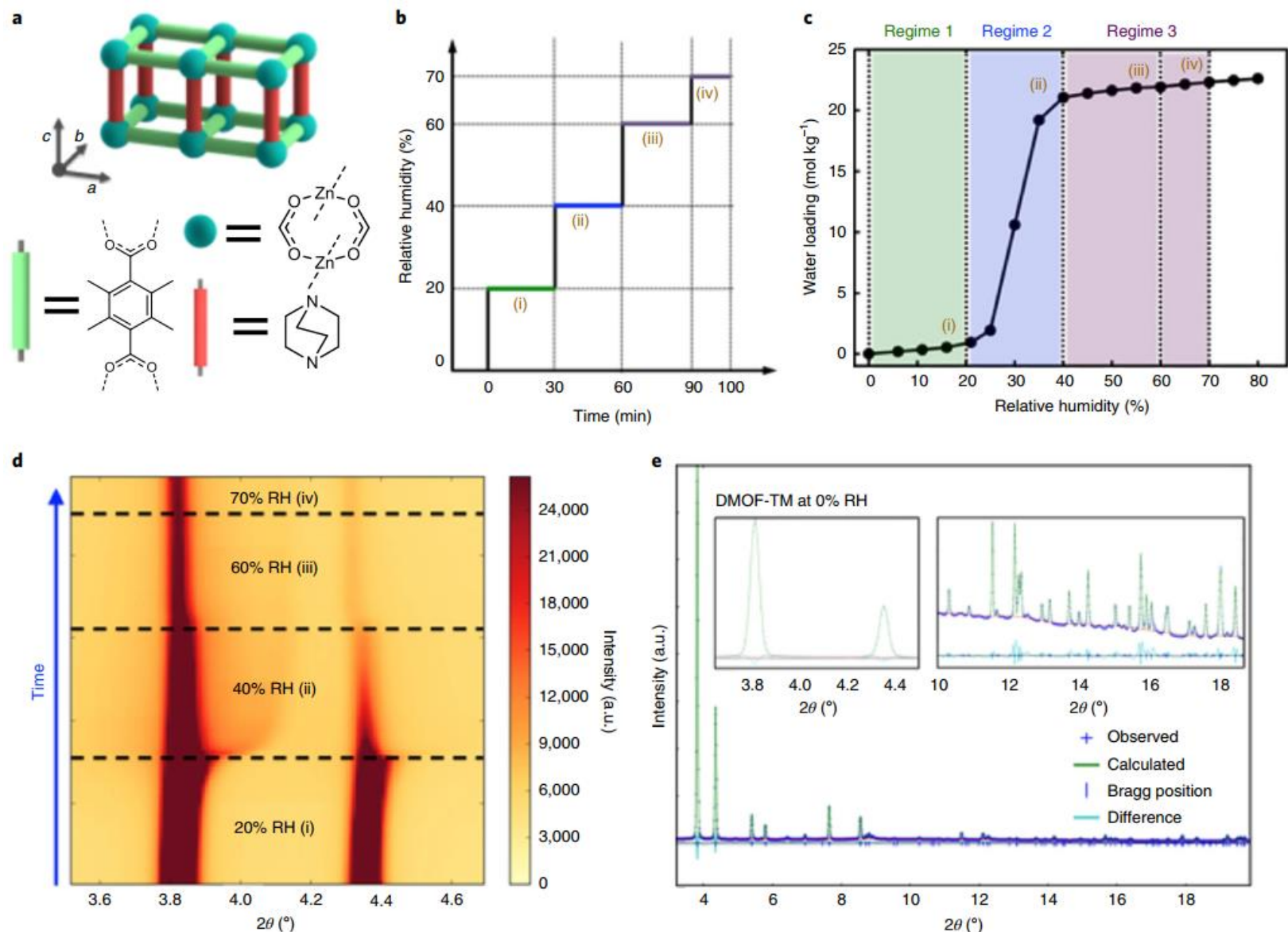


**Fig. 1** | In situ synchrotron powder diffraction experiments. **a**, Structure and schematic representation of the DMOF-TM framework,  $\text{Zn}_2(\text{BDCTM})_2(\text{DABCO})$  and related molecular building blocks: the Zn paddlewheel cluster (dark green) and the two linkers, **BDC-TM** (light green) and **DABCO** (red). **b**, Humidity exposure conditions as a function of time throughout the in situ powder diffraction experiment. **c**, Equilibrium water loadings in DMOF-TM under different humidity conditions at 298 K, with points (i)–(iv) indicating the equilibrium water loadings expected under the in situ exposure conditions shown in **b**. **d**, Evolution of the (110) and (001) Bragg peaks for DMOF-TM with moisture exposure and time ( $\lambda = 0.72768 \text{ \AA}$ ). **e**, Rietveld fit for the  $P4/nbm$  space group DMOF-TM structure with selected low and high  $2\theta$  regions magnified (insets).

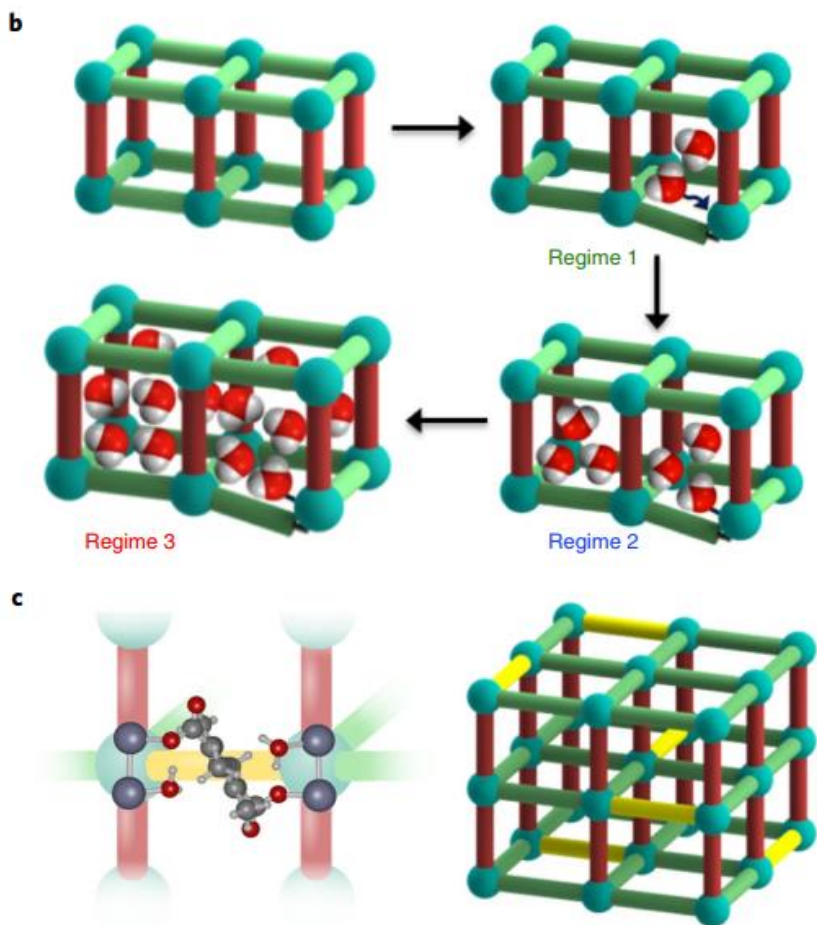
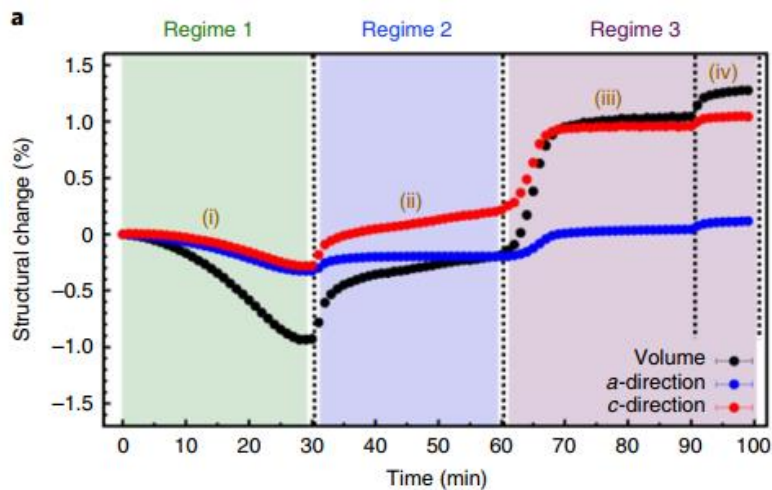
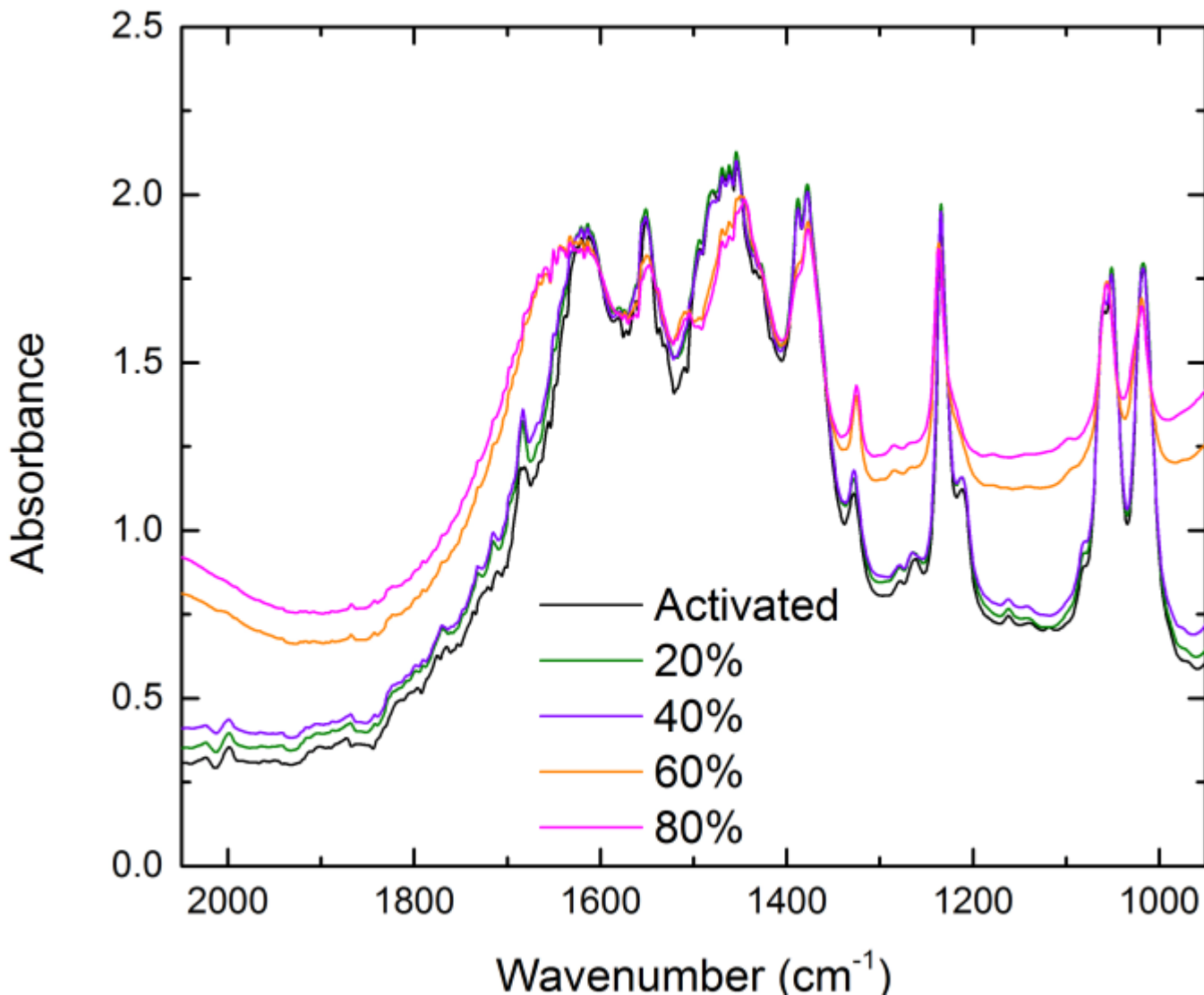


**Fig. 2 |** Water-induced structural changes. **a**, Evolution of crystallographic structural parameters as a function of time and moisture content from in situ powder diffraction experiments. **b**, Schematic of the water-loading process's impact on the experimental crystallographic parameters and structure, as evidenced from XRD and IR experiments. **c**, Depiction of a proposed defect scenario consistent with SCXRD and IR spectroscopy data where unidentate carboxylate defects are generated from the insertion of water molecules in a *cis* fashion at opposite paddle-wheel sites (shown in yellow). Colour code as per Fig. 1; for the water molecules and defect shown in **c**: C, dark grey; O, red; H, light grey.



**Supplementary Figure 10.** Water loading of DMOF-TM, broadening of the  $\sim 1620\text{ cm}^{-1}$  peak indicates the effect of guest water on the framework. Elevation of the baseline of the 60 and 80 %RH spectra indicate an effect of the interstitial water on the framework.



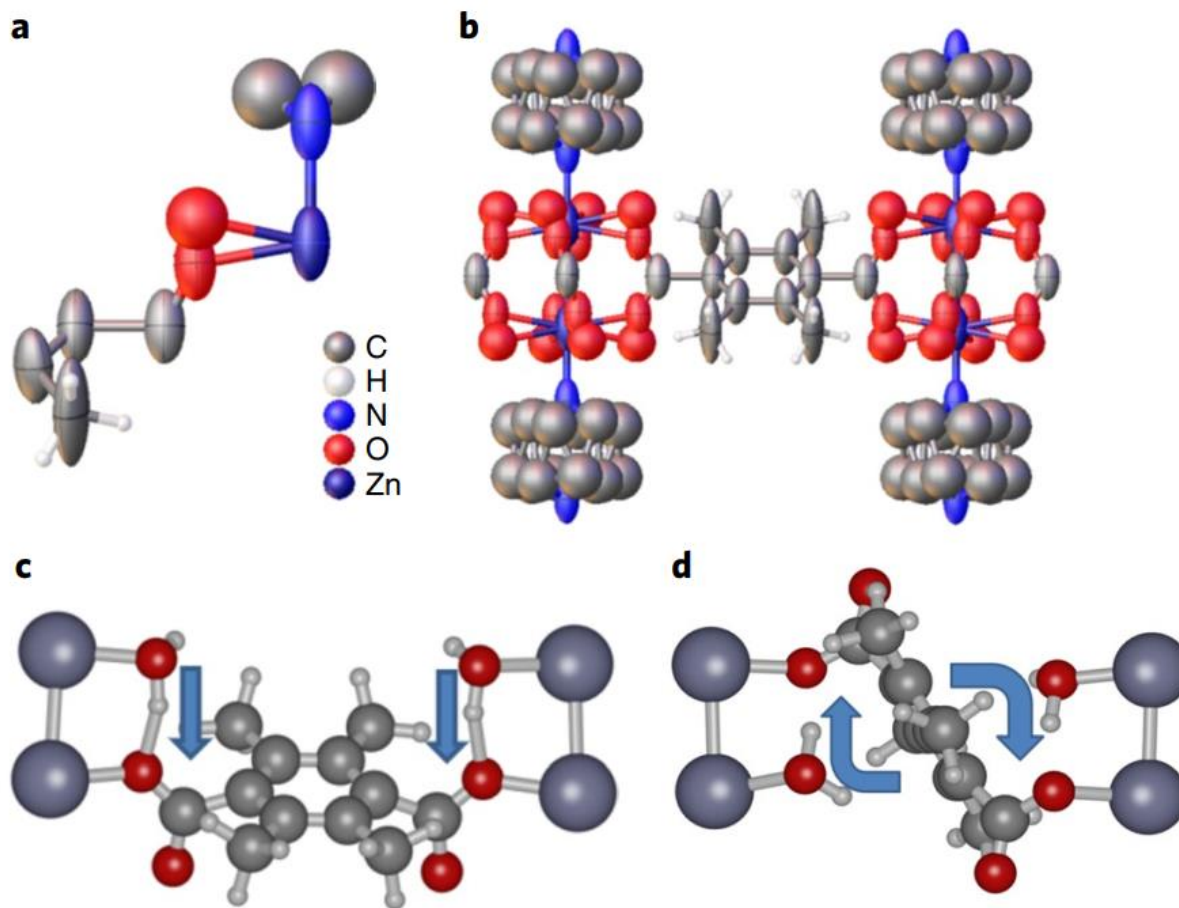


**Fig. 3** | Defect structures. **a**, Asymmetric unit of the SCXRD structure of the defective DMOF-TM. Partial occupancy of water-induced defects above the carboxylate oxygen. **b**, Expanded asymmetric unit detailing a single **BDC-TM** linker, two Zn paddle wheels and four pillaring **DABCO** linkers. Defect oxygen atoms are present at all sites by symmetry. **c,d**, Proposed *cis* (**c**) and *trans* (**d**) defect structures. As indicated by the arrows, quantum mechanical calculations (Supplementary information, theoretical defects calculations) support the *cis* defect structure forming due to a water-induced translation of the linker, whereas the *trans* defect structure originates from a water-induced linker rotation.



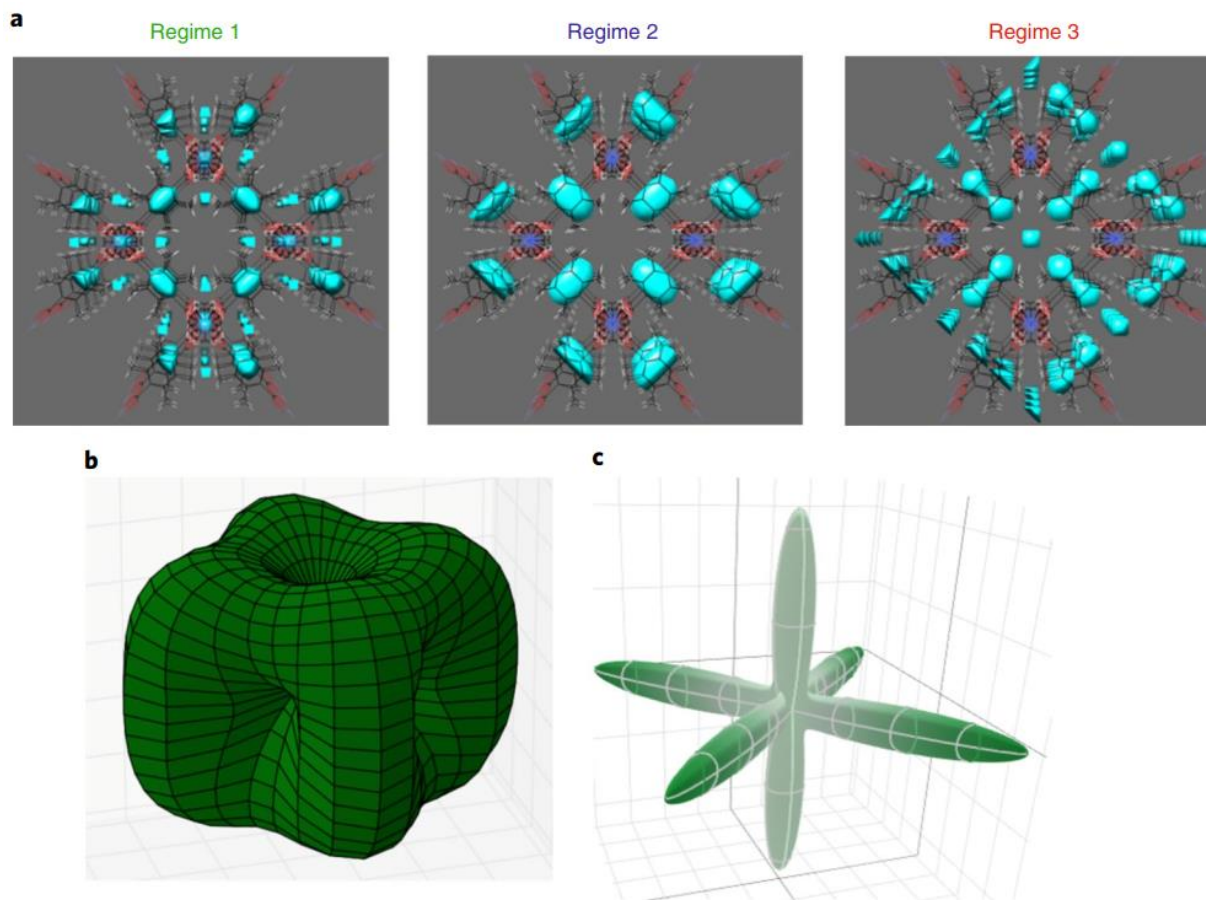


**Fig. 4** | Water siting, microstrain and Young's modulus analysis. **a**, Representative difference envelope density plots generated from the most intense low-index diffraction reflections to show water siting in the crystallographic  $c$  direction. At low water loadings (regime 1), the maximum water density is between the terephthalate and **DABCO** linkers in the structure and, as water loading increases (regimes 2 and 3), the maximum density spreads away from the linkers and towards the centre of the pore. **b**, Experimental microstrain plot for the evacuated structure, obtained from peak broadening behaviour in the synchrotron powder diffraction data. Microstrain arises from non-uniform lattice distortions that create deviations in  $d$  spacings in a crystallographic plane. **c**, Calculated Young's modulus for the evacuated structure, derived from an analysis of the elastic constant tensor of a DMOF-TM flexible force field framework model. The inverse correlation between this plot and the experimental microstrain of **b** implies that the refinement of (synchrotron) powder diffraction data may be used as a tool for understanding the Young's modulus of MOFs.

# Conclusion

- The DMOF-TM framework has a dynamic and reversible structural response to water guest molecules, observed in changes in the unit cell parameters, microstrain, vibrational spectra and atomic structure.
- The dynamic structural response of the DMOF-TM framework to guest water molecules reveals the importance of studying structures without large-scale structural transitions in greater detail.